LANGMUIR

Article

pubs.acs.org/Langmuir

# Lateral Chain Length in Polyalkyl Acrylates Determines the Mobility of Fibronectin at the Cell/Material Interface

Fatma Bathawab,[†] Mark Bennett,[†] Marco Cantini,*[,†] Julien Reboud,[†] Matthew J. Dalby,[‡] and Manuel Salmerón-Sánchez*[,†]

[†]Division of Biomedical Engineering, School of Engineering, University of Glasgow, Glasgow G12 8LT, United Kingdom

[‡]Centre for Cell Engineering, Institute for Molecular, Cell and Systems Biology, University of Glasgow, Glasgow G12 8LT, United Kingdom

Supporting Information

**ABSTRACT:** Cells, by interacting with surfaces indirectly through a layer of extracellular matrix proteins, can respond to a variety of physical properties, such as topography or stiffness. Polymer surface mobility is another physical property that is less well understood but has been indicated to hold the potential to modulate cell behavior. Polymer mobility is related to the glass-transition temperature ($T_g$) of the system, the point at which a polymer transitions from an amorphous solid to a more liquid-like state. This work shows that changes in polymer mobility translate to interfacial mobility of extracellular matrix proteins adsorbed on the material surface. This study has utilized a family of polyalkyl acrylates with similar chemistry but different degrees of mobility, obtained through increasing length of the side chain. These materials are used, in conjunction with fluorescent fibronectin, to determine the mobility of this interfacial layer of protein that constitutes the initial cell−material interface. Furthermore, the extent of fibronectin domain availability ($III_9$, $III_{10}$, - the integrin binding site), cell-mediated reorganization, and cell differentiation was also determined. A nonmonotonic dependence of fibronectin mobility on polymer surface mobility was observed, with a similar trend noted in cell-mediated reorganization of the protein layer by L929 fibroblasts. The availability of the integrin-binding site was higher on the more mobile surfaces, where a similar organization of the protein into networks at the material interface was observed. Finally, differentiation of C2C12 myoblasts was seen to be highly sensitive to surface mobility upon inhibition of cell contractility. Altogether, these findings show that polymer mobility is a subtle influence that translates to the cell/material interface through the protein layer to alter the biological activity of the surface.

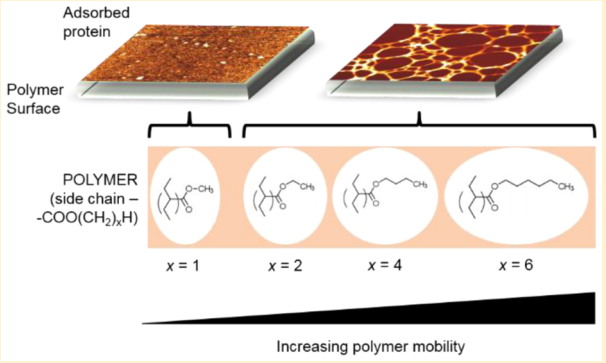


## INTRODUCTION

The cell/material interface has proven crucial to influencing cellular behavior, with substrate topography,[1,2] accessible area/shape,[3] stiffness,[4] dimensionality,[5] and protein tethering[6] known to be some of the physical stimuli perceivable to cells. This ability to control cell fate, without, or with, minimal use of soluble factors, such as growth factors (e.g., BMP-2[7]), is highly sought after in the field of tissue engineering; however, a complete understanding of the mechanisms used by cells to distinguish these physical stimuli is not yet fully understood.[8]

There is emerging evidence that the mobility of the material surface alters cell behavior.[9−13] Different systems have been developed that make use of hydrated mobility, which is the motion of a hydrophilic material interface as a consequence of the interaction with the surrounding water. For example, increasing the tether length of synthetic adhesive peptides to the underlying substrate enhances cell adhesion, cell spreading, and the formation of focal adhesions.[10] PEG-based block copolymers with modulated chain mobility alter fibroblast adhesion and morphology.[11,12] Moreover, model chemistries, tethered to glass with dynamic properties, obtained by controlling side-chain length (number of C), have been shown to influence mesenchymal stem cell (MSC) phenotype.[9] These cell/material interactions involve fluctuating picoscale forces, exerted by cells upon the surface, which can trigger the movement of the polymer surface.[14] It must be noted that the concept of surface mobility is different from surface stiffness. The latter is generally sensed by cells after assembling focal adhesions and probing the surface with nanoscale forces (5.5 nN/$\mu$m$^2$),[15] while surface mobility involves single receptor interactions with much lower and fluctuating forces (picoscale).

Polymers, the chains of which are mobile entities with dynamics directly linked to temperature, are extensively used as biomaterials. Below the glass-transition temperature ($T_g$), the glassy state, polymer chains are almost frozen and movements are mainly restricted to the side groups of the chains at the sub-

Received: August 31, 2015
Revised: December 10, 2015
Published: December 29, 2015

  

DOI: 10.1021/acs.langmuir.5b03259
Langmuir 2016, 32, 800−809

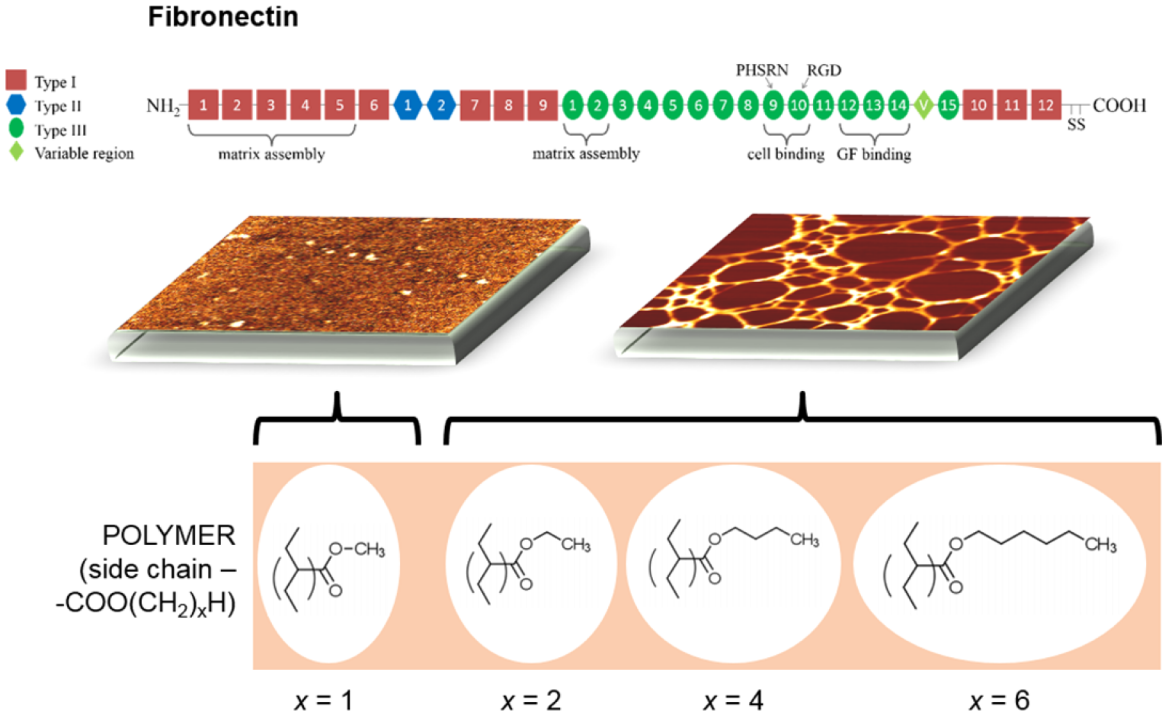


**Figure 1.** Fibronectin and material systems. Conceptual figure of how polymer side-chain length affects the mobility by increasing free volume (represented by the white area) and its effect on the fibronectin layer (monomer shown above). PMA($x$ = 1) leads to adsorption of globular fibronectin, with PEA($x$ = 2), PBA($x$ = 4), and PHA($x$ = 6) all leading to the formation of fibronectin nanonetworks. The fact that the same organization of the protein occurs on these three polymers allows discussion of the effect of surface mobility on protein layers with the same initial conformation/distribution and assessment of the effect of mobility, disregarding major conformational effects of the proteins induced by surface chemistry.

nanometer level. Above $T_g$, a liquid-like state, the free volume drastically increases and polymer chains are highly mobile within distances of tens of nanometers.[16] This is demonstrated conceptually, in the context of this work, in Figure 1. Direct evidence of the scale of these movements can be obtained from experiments in thin polymer films.[17] Varying polymer thickness from 100 to 20 nm leads to monotonically diminished $T_g$, which demonstrates that both film thickness and the movement of polymer chains share the same nanometer range.

Cells interact with surfaces, polymer or otherwise, through a layer of adsorbed proteins using transmembrane integrins, which assemble into large multiprotein complexes called focal adhesions.[18] These allow cells to indirectly detect surface properties by the latter's ability to affect the conformation and flexibility of the extracellular matrix (ECM) proteins, consequently exposing key cell-binding residues on these matrix proteins. A prime example of these types of proteins is fibronectin (FN), a ∼440 kDa dimer protein, which binds predominantly to $\alpha_5\beta_1$ integrins through the RGD and PHRSN (synergy) domains located in repeats $III_{10}$ and $III_9$, respectively[19] (shown schematically in Figure 1). Physiologically, it maintains a globular conformation, but via cellular stimuli it can unfold into an extended conformation, exposing domains responsible for lateral assembly and network formation, thus forming an integral part of the ECM.[20] Previous work has demonstrated that surface chemistry can alter the amount and conformation of FN adsorbed onto materials, determining its bioactivity: Garcia et al., using model surface chemistry, showed that the integrin binding domain of FN can be presented to cells with different biological activity depending on the hydrophilic/hydrophobic balance of the surface.[21] Changes in the protein orientation/conformation, as a consequence of its conjugation to a surface, also translate into an altered activity.[22]

Because cells only can respond to the surface mobility indirectly, via the adsorbed protein layer, it is the aim of this work to observe how *surface mobility* translates into *interfacial mobility* of the protein layer. Among the broad range of available polymers, this work has selected a family of poly(alkyl acrylates), with $T_g$ well below 37 °C (with a vinyl backbone and side groups $-COO(CH_2)_xH$, where $x$ = 1, 2, 4, and 6 for polymethyl, ethyl, butyl, and hexyl acrylates, respectively),[13,23] which interact strongly with FN[24] and on which FN self-assembles into a network of nanofibrils[17] (for $x \geq 2$), as shown in Figure 1. Thus, interface mobility of the protein layer is expected to be directly linked to the mobility of the underlying polymer surface. This work therefore shows that the mobility of hydrophobic polymers (hydration-independent) is a fundamental, dynamic property. This can then be translated into the interfacial layer of adsorbed FN, and this subsequently plays a role in cell adhesion, reorganization, and differentiation.

## MATERIALS AND METHODS

**Fibronectin Labeling.** 1 mg/mL fibronectin from human plasma (Sigma-Aldrich) was labeled using the FluoroTag FITC conjugation kit (Sigma-Aldrich). The protocol provided with the kit was adapted for fibronectin labeling (by adjusting the FN/FITC labeling ratio). In brief, 250 μL of 1 mg/mL fibronectin was incubated with FITC in a fluorescent molecule to protein ratio of 125:1 for 2 h. The labeled fibronectin was then separated from unconjugated molecules via a G-25 Sephadex column. The success of the conjugation procedure was determined by measuring the absorbance of the retrieved fractions at


DOI: 10.1021/acs.langmuir.5b03259
Langmuir 2016, 32, 800−809

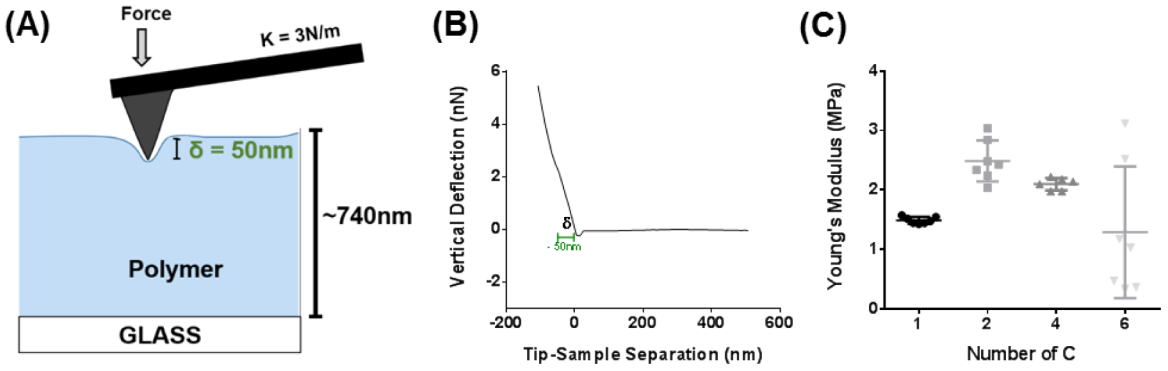


**Figure 2.** Nanoindentation of polymer films. (A) Sketch of nanoindentation showing cantilever indenting a polymer surface. (B) Force curve from measurements, showing an example of the initial 50 nm indentation of a polymer surface ($\delta$), on which the Hertz model was applied to calculate the Young's moduli. (C) Young's moduli of polymer films; each point on the graph is an average derived from 64 measurements (per sample).

280 (protein) and 495 nm (FITC) and calculated using equations provided.

**Surface Preparation and Protein Adsorption.** Polymers were synthesized by radical polymerization of acrylate monomers using 1 wt % benzoin. Polyacrylate solutions were prepared by dissolving bulk polymers in toluene, with a 4% w/v solution for PMA and PEA and a 6% w/v solution for PBA and PHA. 12 mm diameter glass coverslips were cleaned by sonication in ethanol and dried at 60 °C. 100 $\mu$L of polymer solution was added to the surface and spin-coated for 30 s at 3000 rpm. Residual solvent was removed by drying at 60 °C in vacuum for 1 h. Polymer surfaces were coated with a 20 $\mu$g/mL fibronectin solution in DPBS for 10 min (for AFM studies) or 1 h (for domain availability, mobility measurement, and cell culture). They were then washed in DPBS and Milli-Q water and in the case of AFM studies dried with $N_2$. This difference in time is to aid in the imaging of the network via AFM, which can reduce in clarity at higher time points due to adsorption of more protein.

**Surface Characterization.** Phase images were obtained for coated and uncoated polymer surfaces via AFM in AC mode (Nanowizard 3 Bioscience AFM, JPK). A pyramidal silicon nitride tip, with a cantilever spring constant of ~3 N/m and a resonance frequency of 75 kHz (MPP-21120, Bruker), was used. Fractal dimension analysis was carried out on the images of FN-coated samples using the ImageJ Fractal box count analysis tool, using box sizes of 2, 3, 4, 6, 8, 12, 16, 32, and 64 pixels. Force spectroscopy curves were obtained, after calibration of tip sensitivity and spring constant, with a set-point of 10 nN, a zeta length of 10 $\mu$m, a constant duration of 1 s, and at room temperature. Analysis was performed using the JPK processing software (v4.3.21), and force curves were fitted with a Hertz model at 50 nm indentation. The water contact angle of the adsorbed protein surfaces was measured both statically and dynamically, with the latter providing the hysteresis angle of the surface (Optical Tensiometer Theta, Biolin Scientific). Static angles were measured using the sessile drop method with 3 $\mu$L drops. Advancing angle was measured by adding water to the original static volume and receding by removing it at a rate of 0.1 $\mu$L/s.

**Determining Protein Mobility.** Photobleaching was performed on the fluorescent, protein-coated surfaces, with the four polymers and glass as a control on an Olympus FV1000. The samples were stored at 37 °C (under cell culture conditions), and the fluorescence signal was measured over a period of 120 h using a Zeiss Observer Z.1 widefield microscope. A 20 × 50 $\mu m^2$ area was selected manually across the bleach border region (Figure 6A). Using ImageJ, a surface intensity profile was obtained, where each column of pixels (for one value of $x$) was averaged, yielding a line graph (Figure 6B) across the edge of the bleached area. To quantify the changes, using OriginPro 8, the center of the linear region was taken as the central point of the selection area ($x$ = 10 $\mu$m), and a linear fit over 0.5 $\mu$m (1 $\mu$m total) on either side of this point was used to determine the linear gradient for each time point (Figure 6B, red line). For each time point, the gradient of the fluorescence intensity across the border was obtained (Figure 6C), which was then fitted with an exponential growth (over time), shown in eq 1.

$$Y = Y0 \times e^{(k \times t)} \quad (1)$$

where $Y0$ is the $Y$ value at time zero, $k$ is the rate constant, and $t$ is time.

**Quantifying Domain Availability.** The availability of FN adsorbed on polymer surfaces as well as that of the RGD and synergy domains was determined by ELISA. Samples were blocked for 30 min with 1% w/v BSA (Sigma-Aldrich). To determine the availability of FN, we incubated rabbit polyclonal anti-FN antibody (Sigma-Aldrich, 1:10 000) for 1 h, followed by a 1 h incubation with biotinylated horse antirabbit secondary antibody (Vectorlabs, 1:10 000), both at room temperature (RT). Samples were then incubated with HRP-streptavidin (R&D Systems) for 20 min, washed, and incubated with HRP substrate (R&D Systems) for 20 min. After stopping the reaction, using the stop solution, absorbance was measured at 450 (maximal absorbance of the tag) and 540 nm (blank control, to determine background absorbance). To assess the availability of cell-binding domains, we incubated samples at RT with monoclonal mouse primary antibody (mAb1937, 1:20,000 in 1% BSA or HFN 7.1 antibody for the synergy or RGD domain, respectively). The samples were then washed with 0.5% Tween 20 and incubated with goat antimouse HRP-tagged secondary antibody (1:10 000 in 1% BSA solution) for 1 h (RT). After washing with 0.5% Tween 20, samples were incubated with HRP substrate solution in the absence of light for 20 min. The reaction was terminated with stop solution (R&D Systems) and absorbance was measured.

**Cell Studies.** L929 fibroblasts and C2C12 myoblasts were cultured in DMEM (1×) Dulbecco's modified Eagle medium (+ 4.5 g/L D-glucose, + L-glutamine, Gibco), containing 1% antibiotic mix of penicillin and streptomycin and 10% (L929) or 20% (C2C12) FBS (Gibco). To observe cell-mediated protein reorganization, we seeded cells on fibronectin-coated coverslips, within a 24-well plate, on glass and polymer surfaces at a density of ~5000 cells/$cm^2$ in the presence of 10% FBS. After incubating for 3 h cells were then fixed with 3.7% formaldehyde for 20 min (4 °C). The cells were subsequently permeabilized with 0.1% Triton X-100 for 5 min. They were blocked with 1% BSA for 20 min then stained for actin for 1 h with rhodamine phallotoxin R415 (Life Technologies, 1:40). Actin (stained with R415) was used as a mask for the reorganization of the underlying FN layer within the cell areas and determining the morphological characteristics of the cell. For the studies of the differentiation of C2C12, cells were diluted in differentiation medium (DMEM 41965 + 1% PS + 1% ITS-X) and seeding was performed on coated surfaces at 18 500 cells/$cm^2$. After 3 h the media was refreshed with differentiation medium and blebbistatin was added to experimental samples at 10 $\mu$M. After 4 days samples were washed and fixed (20:2:1 EtOH 70%/formaldehyde 37%/acetic acid) for 10 min (4 °C). Cells were then incubated with 5% goat serum for 1 h (RT). Subsequently, cells were incubated with antisarcomeric myosin antibody (1:250), followed by Cy3 antimouse


DOI: 10.1021/acs.langmuir.5b03259
Langmuir 2016, 32, 800−809

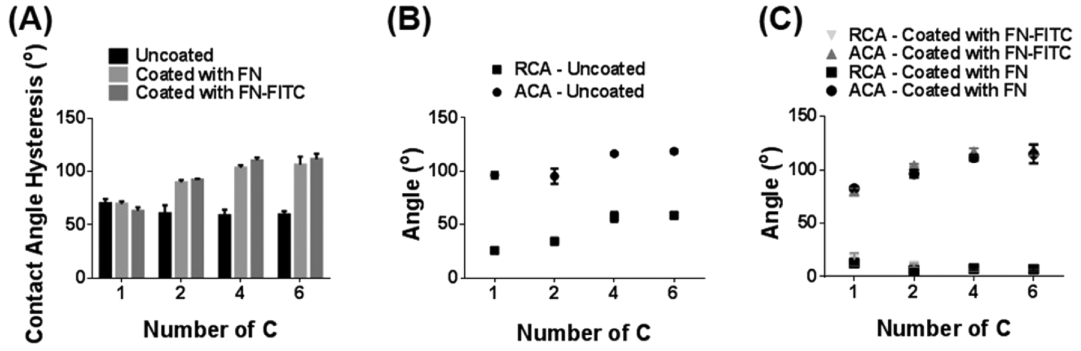


**Figure 3.** Surface hydrophilicity. Dynamic water contact angles were measured on the polymer surfaces before and after coating with a FN solution of concentration 20 $\mu$g/mL. (A) Contact-angle hysteresis. (B) Advancing (ACA) and receding (RCA) angles of the uncoated polymer surface and (C) of the surfaces after coating with FN and labeled FN.

antibody (1:200), both for 1 h at 37 °C, in the absence of light. In all instances, DAPI-containing mounting media was added to stain for nuclei.

**Data Analysis.** All images were analyzed using ImageJ software[25] (v1.48). The data were statistically analyzed using GraphPad Prism 6. Where relevant, one-way ANOVA tests were performed to determine any statistically significant differences: $^{*}p \leq 0.05$, $^{**}p \leq 0.01$, $^{***}p \leq 0.001$, and $^{****}p \leq 0.0001$ (GraphPad software, La Jolla, CA). The linear gradient of bleaching analysis was determined in OriginPro 8 (OrginLab, Northampton, MA), with this subsequently being transferred to and analyzed in GraphPad Prism 6.

## RESULTS

**Surface Characterization and Protein Adsorption.** In this study four polymers with similar physicochemical properties, each comprising a vinyl backbone with a side group $-COO(CH_2)_xH$ ($x = 1$, $x = 2$, $x = 4$, and $x = 6$), were used. The spin-coated surfaces were found to be smooth, with similar root-mean-square (RMS) roughness of $\sim 37.5 \pm 5.5 \times 10^1$ pm and thickness of $7.4 \pm 2.3 \times 10^2$ nm, regardless of composition. Furthermore, AFM nanoindentation determined that all surfaces had Young's moduli $\geq$1 MPa, greater than the 40 kPa stiffness threshold that cells can detect[15] (Figure 2).

Measurement of the water contact angle of these polymer surfaces, with and without FN coating, as well as comparing the labeled and unlabeled protein, allowed for a further understanding of the physical characteristics (Figure 3). There was a minimal change in the contact-angle hysteresis (hysteresis = advancing angle − receding angle, Figure 3) and in the static contact angle (SCA) (Supplementary Figure S1), with increasing polymer chain length in the absence of fibronectin (Figure 3A); however, both advancing and receding angles were seen to increase, with increasing side chain length (Figure 3B). Coating the polymers with FN led to a decrease in the receding angles, with a concomitant increase in the advancing angles (Figure 3C). Furthermore, there was no change in the wettability properties when labeled FN was used compared with that of the unlabeled protein (Figure 3A).

Phase imaging of tapping mode AFM, with fractal dimension analysis, showed that FITC labeling of the FN protein did not affect the distribution and conformation adopted by FN upon adsorption on the different surfaces (Figure 4). With or without the FITC label, it was noted that network formation did not occur on PMA ($x = 1$), where globular aggregates were observed, while PEA ($x = 2$), PBA ($x = 4$), and PHA ($x = 6$) surfaces supported the formation of fibrillar protein networks;[23] with longer adsorption times, the network structure is maintained and becomes denser (Supplementary Figure S2).

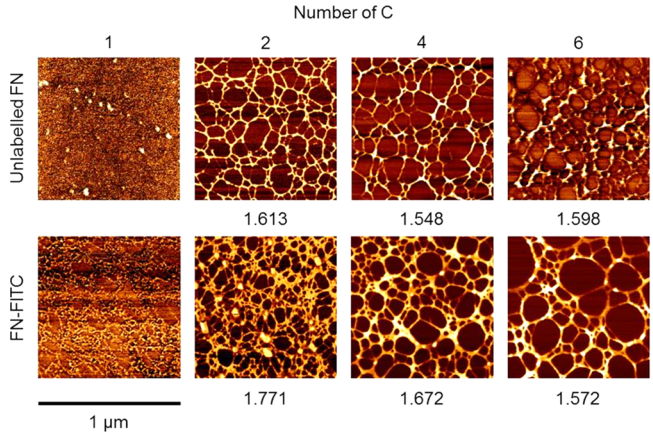


**Figure 4.** Atomic force microscopy. Fibronectin distribution on the polymer surfaces by AFM (AC mode) after adsorption from a solution of concentration 20 $\mu$g/mL. FN is organized into nanonetworks on PEA ($x = 2$), PBA ($x = 4$), and PHA ($x = 6$). These 1 $\mu$m × 1 $\mu$m phase images demonstrate the similarities in protein distribution in the labeled and unlabeled forms. The values shown underneath the network forming polymers relate to the fractal dimension (D), a descriptor of the complexity of a pattern that accounts for the network connectivity.

This indicates that FITC is an appropriate means through which to analyze the interfacial mobility of FN and how this property relates to domain availability and cell-mediated reorganization.

**Quantification of the Protein Layer.** The surface density of FN, as quantified by the BCA assay, shows similar adsorbed levels on each surface (Supplementary Figure S3). The adsorbed FN (regions of interest shown schematically in Figure 5A) was further characterized in terms of its availability on the material surface, considering both general availability of the protein and the specific availability of key domains for cell binding.[26] Figure 5B shows that the availability of the adsorbed FN, determined via polyclonal antibody binding, decreases on the more mobile surfaces. Importantly, in contrast with this, the availability of the cell-binding domains, the RGD (Figure 5C) and PHSRN (synergy) sites (Figure 5D), as indicated by the arrows in Figure 5A, was observed to increase on the more mobile, network-forming, polymers.

Polymer surfaces coated with FITC-labeled FN were used to measure the interfacial mobility of the protein layer adsorbed onto this family of polymers (Figure 6). Specifically, by bleaching large areas of each of the protein-coated polymer


DOI: 10.1021/acs.langmuir.5b03259
Langmuir 2016, 32, 800−809

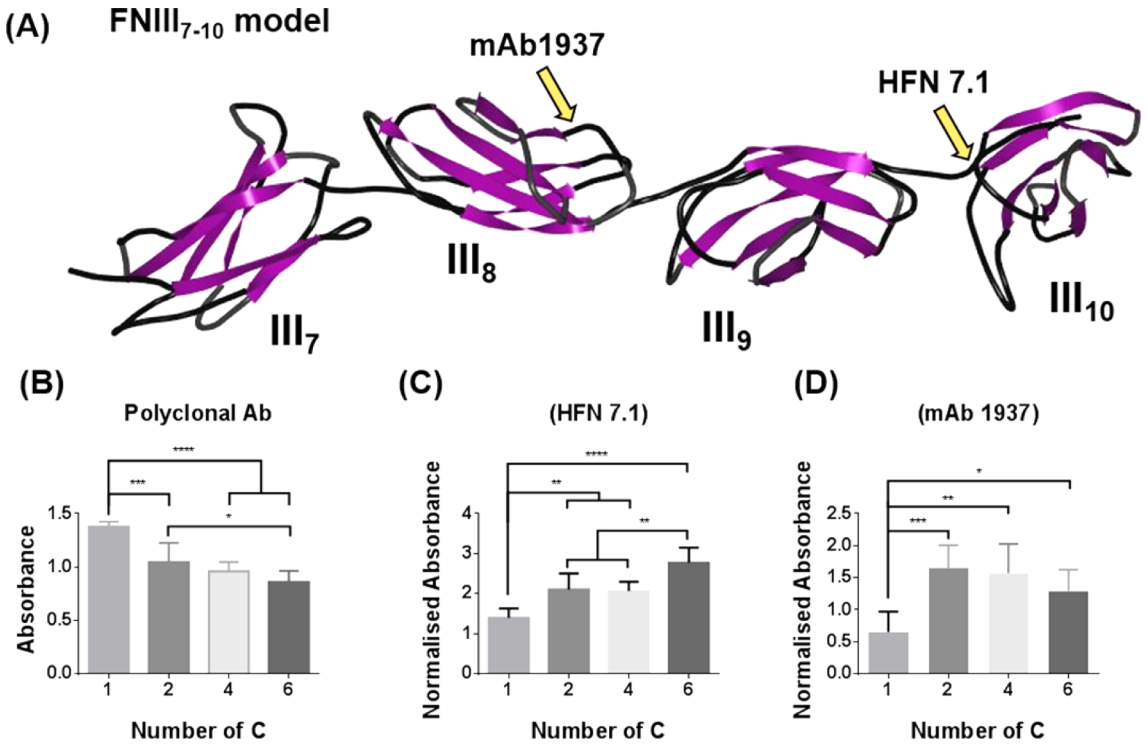


**Figure 5.** Fibronectin conformation. Exposure of epitopes of FN when adsorbed on polymer surfaces from a solution of concentration 20 $\mu$g/mL. (A) $FNIII_{7-10}$ model with arrows pointing to binding sites for mAb1937 and HFN 7.1. Image from the RCSB PDB (www.rcsb.org)[26] of PDB ID 1FNF. (B) Overall availability of FN using a polyclonal antibody. (C) RGD cell-binding site exposure (HFN 7.1 Ab). (D) Exposure of the synergy site (mAb 1937 Ab). Panels C and D were normalized using panel B.

surfaces, the long-term change in the surface fluorescence intensity profile was measured. FN mobility is linked to the fluorescence recovery into the bleached area, together with movement of "dark" species into the untreated area, resulting in a local change in the fluorescence signal. The focus here was upon the edge of the bleached region due to the small length scale of surface mobility limiting the effects to this boundary region (Figure 6A). The linear fit of the central region, as defined by the 1 $\mu$m region spanning the central point of the selection area ($x$ = 10 $\mu$m, detailed further in methods), provided a gradient, plotted for each time point (Figure 6B). An exponential growth (eq 1) to the variation of this gradient value over time was fitted and used as an indicator of the mobility of the protein layer (Figure 6C).

A nonmonotonic dependence of the interfacial mobility of the fibronectin (as indicated by $k$, the rate constant) adsorbed onto the surface, with respect to the mobility of the polymer (represented by their glass-transition temperatures), was observed (Figure 6D,E). Upon increasing polymer mobility, at 37 °C, from PMA ($T_g \approx 10$ °C) to PEA ($T_g \approx -20$ °C), a reduction in FN interfacial mobility was observed. Upon further increasing polymer mobility to PBA ($T_g \approx -50$ °C), the FN mobility returns to be similar to that seen on PMA, and for PHA ($T_g \approx -70$ °C) a significant increase in FN mobility was observed.

**Cell-Mediated FN Reorganization and Cell Differentiation.** All surfaces coated with FN supported attachment of L929 fibroblasts. Cells were well spread on the protein-coated polymers and the glass control after 3 h. Well-developed cytoskeletons were observed in all cases, and no significant differences in cell size and shape were noted (Supplementary Figure S4). The use of FITC-labeled fibronectin permitted the observation of the extent of cell-mediated reorganization of the adsorbed protein layer without the complication of cell-secreted fibronectin being taken into account. Figure 7A shows the difference in the relative intensity of fibronectin underneath the cell area as compared with the area outside the cell. Indeed, this difference in the intensity of fluorescence coming from FN beneath or outside the cell area can readily be observed on all of the protein-coated surfaces (Figure 7B). Not only can reorganization be seen but also the labeled FN indicates where the cell is exerting the greatest amount of force on the surfaces, indicated by the brighter and darker areas, where FN is accumulated or taken from, respectively. This semiquantitative approach allowed for the determination of a trend in the extent of cell-mediated protein reorganization on each of the surfaces. PMA ($x$ = 1) and PEA ($x$ = 2) showed the smallest extent of cell-mediated reorganization, with FN reorganization increasing with the mobility of the protein layer. Cells on PHA allowed for the highest extent of FN reorganization, thus replicating the trend of the mobility of the protein layer (Figure 6C).

Finally, C2C12 cells (mouse myoblast cells capable of differentiating into mature myotubes in vitro) were used to assess the ability of these polymer−protein interfaces to induce cell differentiation (Figure 8), with col I used a standard control for differentiation. The highest levels of differentiation were seen on PEA ($x$ = 2) and PBA ($x$ = 4), with the level of differentiation reducing on PHA ($x$ = 6) (Figure 8A). Inhibition of cell contractility using blebbistatin, a myosin inhibitor, adversely affected C2C12 cell morphology and differentiation (Figure 8B). Interestingly, inhibiting the cells' ability to exert force produced a trend opposite to that of the protein mobility.


DOI: 10.1021/acs.langmuir.5b03259
Langmuir 2016, 32, 800−809

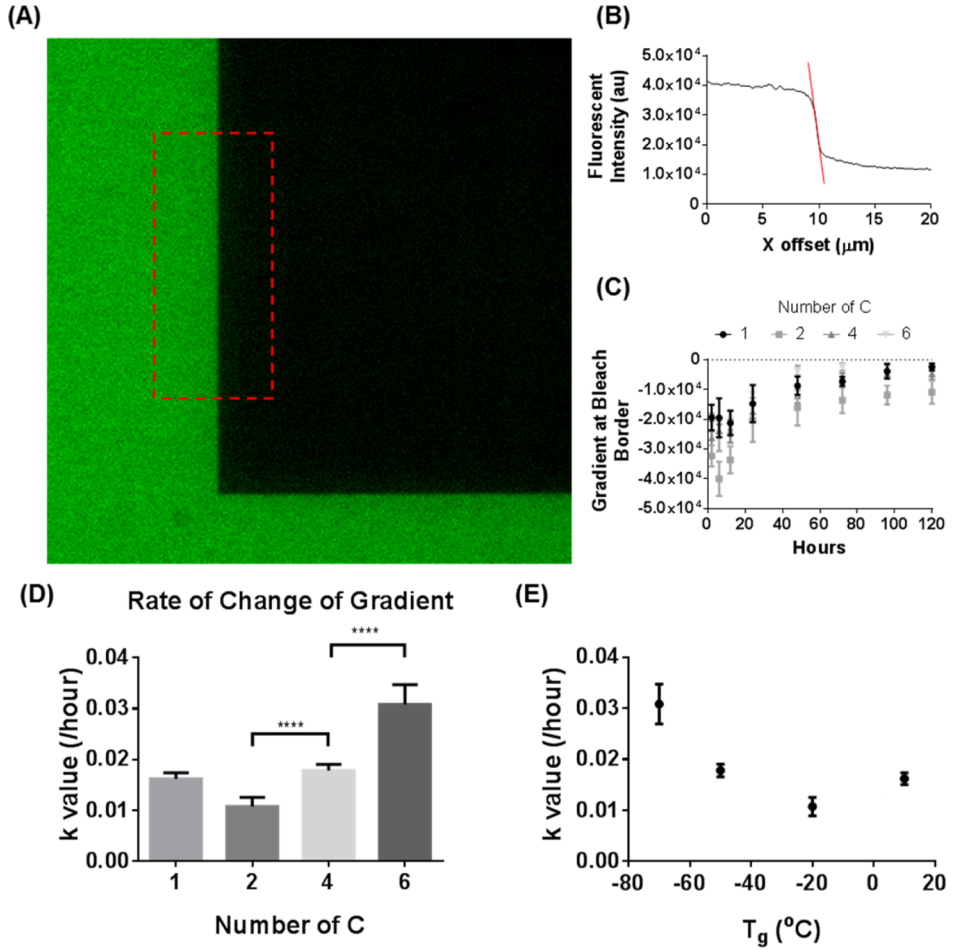


**Figure 6.** Interfacial mobility. Measuring the rate of change in fluorescence intensity profile as an indicator of protein mobility. (A) Bleach border region, with the manually selected area highlighted. (B) Linear gradient value of the bleach border used to determine any changes of the intensity profile at each time point. (C) Comparison of the gradient value at each time point ($N$ = 10) for each of the polymer surface. This is then used to determine the rate constant ($k$ value) of the exponential growth equation. (D) Gradient of the linear region of the bleach border changes with respect to time for each of the polymers. (E) Ascertained $k$ values compared with the glass-transition temperature, $T_g$, of the polymers.

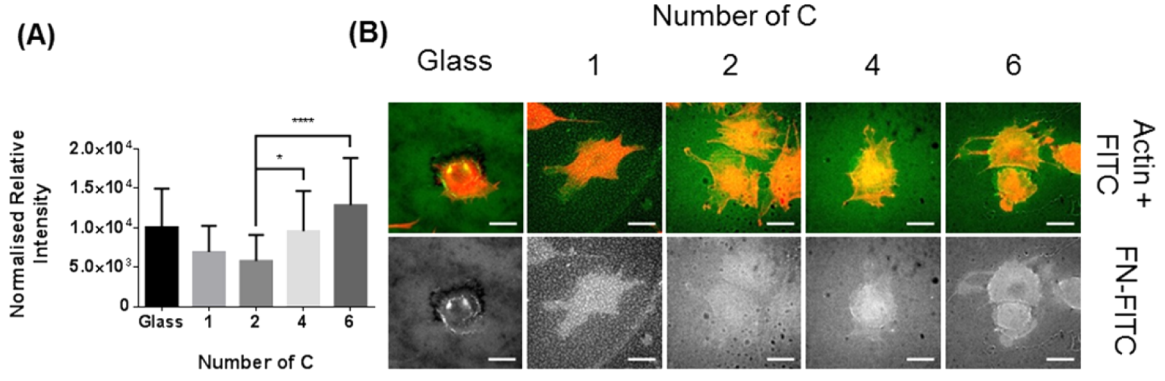


**Figure 7.** FN reorganization. Cell-mediated FN reorganization on differently mobile polymer surfaces. (A) Relative differences in the fluorescence intensity within the cell area (as defined by the stained actin) compared with outside the cell area. (B) Cell (actin, red) with the corresponding fibronectin layer (green) below for glass, PMA ($x$ = 1), PEA($x$ = 2), PBA($x$ = 4), and PHA($x$ = 6), respectively (scale bar = 25 $\mu$m).

## DISCUSSION

Previous work has shown that polymer surface mobility affects the cellular response in a nonmonotonic fashion.[13,27,28] It has been shown by a number of groups that surface mobility, in various forms, can have a profound effect on cellular attachment,[10] morphology,[12] and response.[29,30] This new work has sought to directly relate how the observed protein mobility and organization at the cell/material interface, determined by the polymer surface mobility, influences the cellular response.

**Physical Properties of the Surfaces.** The set of polymers presented here differ only slightly in their side-chain chemistry by the sequential addition of methyl groups. As previously mentioned, all surfaces were above the detectable stiffness



DOI: 10.1021/acs.langmuir.5b03259
Langmuir 2016, 32, 800−809

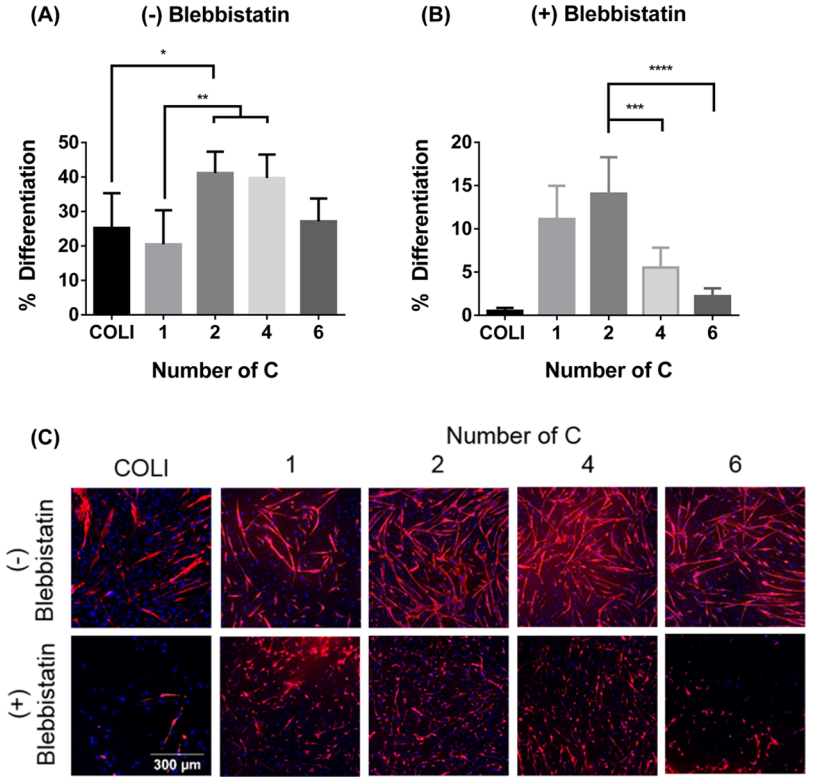


**Figure 8.** Cell differentiation. Differentiation of C2C12 cells cultured on FN coated Collagen I, PMA, PEA, PBA, and PHA (A) without and (B) with a contractility inhibitor (blebbistatin). COLI is the differentiation control, and the percentage of differentiation is measured as the ratio of sarcomeric myosin-positive cells. (C) Representative pictures: nuclei (blue) and sarcomeric myosin (red) for each of the surfaces. In panel B there was significant differences between COLI and polymer surfaces with 1,2 ($p$ = ****) and 3 ($p$ = *) carbons in the side chain.

threshold of the cells, despite variation (Figure 2). The large variation in Young's modulus seen in PHA ($x$ = 6) can be attributed to the adhesive nature of this polymer. Minimal differences in wettability of the untreated polymer surfaces, by observation of the static contact angles (Supplementary Figure S1), were noted. Contact-angle hysteresis was also similar on all surfaces and increased after FN coating (Figure 3A). The advancing angle of the protein-coated surface was seen to increase with increasing side chain length and mobility of the polymer, while the opposite was seen to be true in the case of the receding angle (Figure 3C). These differences in dynamic contact-angle measurements reveal a different state of the adsorbed protein, suggesting an increase in protein surface coverage from PMA ($x$ = 1) to the rest of the polymers (compatible with the unfolding of the protein and the formation of fibrils, Figure 4). On the more mobile, protein network-forming polymers ($x \geq 2$), the increase in contact angles hysteresis indicates an enhanced ability of the adsorbed protein to undergo molecular rearrangement at the water/air interface, which is compatible with an increased mobility of the protein layer. This increase in the hysteresis was noted in both polymers coated with labeled and unlabeled FN (Figure 3A), indicating that both have similar physical properties.

This is supported by data shown in Figure 4, which shows that the conformation of the adsorbed protein changes drastically between PMA ($x$ = 1) and PEA ($x$ = 2)[23,31] (and the rest of the more mobile polymers). This conformational change, from globular to fibrillar, is believed to be driven by the orientation of key hydrophobic residues to interact with the polymer backbone.[32] This leads to the exposure of FN-FN binding sites, which in turn drives further conformational changes through electrostatic and entropic factors.[33] Of key importance is the fact that there appears to be minimal differences between the labeled and unlabeled FN after adsorption on material surfaces, which would preclude its use in these studies. Furthermore, measurement of the fractal dimension of the network-forming surfaces ($x \geq 2$), as seen in Figure 4, shows minimal differences in conformation and complexity of the protein networks. This implies that the contribution of protein conformation in the bioactivity of these protein networks is not likely to be a significant factor.

While previous work has shown that the stiffness of a substrate[4] can affect cellular behavior, this can be discounted here in favor of surface mobility. For the elasticity/stiffness of the ECM to play a role in cell response, both must be in the same order of magnitude. The range of moduli previously reported is within the range ~1 to 40 kPa,[4] which is within the range of stress that cells are able to exert on a surface; the maximum force is reported to be between 1 and 5 nN $\mu m^{-2}$ (kPa).[15] The stiffness of these surfaces, as determined by nanoindentation, is shown to be in the megapascal range (Figure 2); hence cells should not be able to deform the underlying substrate.

Further evidence of this lies in the lack of difference in cell morphology (specifically size, Supplementary Figure S4), which has previously been observed to change upon detection of substrates with different mechanical properties.[34] Furthermore, the cytoskeleton was not seen to be arranged differently, which is also expected if the cell can detect the mechanical properties of the surface.[35] Finally, the traction forces exerted by a cell on the surface are dependent on the stiffness of a surface.[35] These traction forces change in relation to the size of focal adhesions,


DOI: 10.1021/acs.langmuir.5b03259
Langmuir 2016, 32, 800−809

which is also not seen to change here (Supplementary Figure S5).[36] Further factors, such as surface roughness, have been shown to have implications in cell behavior;[37,38] this, too, can be discounted because this parameter is similar (RMS roughness ~37.5 ± 5.5 × $10^1$ pm) on all surfaces. The fact that these surfaces (PEA ($x$ = 2), PBA ($x$ = 4), PHA ($x$ = 6)) have similar physical and chemical properties allows the attribution of any differences in cell behavior to subtle changes in surface mobility of the polymers.

**Fibronectin Availability.** The overall availability of FN and its domains (shown schematically in Figure 5A)[26] on the polymer surfaces after adsorption changes for the different surfaces, decreasing with increasing side-chain length (Figure 5B). This may be related to the unfolding of FN, meaning that single molecules occupy a greater surface area. In contrast, the availability of the adhesion tripeptide, RGD, was seen to increase on the network-forming surfaces (PEA ($x$ = 1), PBA ($x$ = 4), PHA ($x$ = 6)) (Figure 5C). This demonstrates that the unfolding of FN, due to surface interactions, should positively alter cell adhesion. The availability of the synergy site (PHSRN) was seen to be significantly elevated on network-forming surfaces, with no significant differences between PEA ($x$ = 2), PBA ($x$ = 4), and PHA ($x$ = 6) (Figure 5D).

As previously alluded to, it has been established, in previous work, that the conformation of the protein layer can be affected by surface chemistry.[21] Furthermore, it has been shown that the orientation of the fibronectin molecules attached to the surface can have an effect on their bioactivity.[22,23] The conformational change of FN upon adsorption onto PMA ($x$ = 1) versus the rest of the polymers ($x \geq 2$) observed via AFM (Figure 4) is reflected on the different domain availability measured by ELISA (Figure 5) and leads to a different bioactivity of the protein layer.[23,31] On the more mobile polymers ($x \geq 2$), the conformation and domain availability of FN upon adsorption is seen to be comparable (Figure 5). This suggests that whereas conformation plays a role in the change of FN activity between PMA and PEA, the mobility is the dominant factor behind the differences in cellular response on the protein network-forming surfaces (Figures 7 and 8).

**Translation of Surface to Interfacial Mobility.** It is well-established that cells interact with surfaces through an interfacial layer of extracellular matrix proteins (e.g., FN).[39] Furthermore, it has been hypothesized that polymer surface mobility can be translated through this protein layer, subsequently being detected by cells.[13] Determination of the mobility of the adsorbed protein on the polymer surface, via fluorescence recovery of the bleach border region, has provided an unexpected result, where the interfacial mobility does not correlate directly with glass-transition temperature (polymer mobility). Previous work has shown that the mobility of polymer chains at specific temperatures increases as the glass-transition temperature, $T_g$, decreases.[40] Therefore, at 37 °C, polymer surface mobility will increase with direct proportionality to side-chain length, that is, mobility increasing from PMA($x$ = 1) < PEA($x$ = 2) < PBA($x$ = 4) < PHA($x$ = 6). One would thus expect that when the interaction of the protein with the underlying polymer surface is strong enough, as is the case of this family of polymers, the mobility of the protein layer would be a reflection of that of the material surface; however, a nonmonotonic dependence of protein mobility on polymer mobility was noted.

It is believed that the initial decrease in FN mobility between PMA ($x$ = 1) and PEA ($x$ = 2) is due to the observed formation of a FN nanonetwork on the PEA surface, compared with the globular conformation on PMA surfaces. The network is likely formed through interaction with the PEA (and PBA and PHA surfaces) providing access to the 70 kDa amino-terminal fragment $I_{1-5}$, which is vital to matrix formation.[20] It can be postulated that network formation may restrict the freedom of motion of the protein, thus reducing mobility. Upon further increase in the polymer mobility (PBA ($x$ = 4) and PHA ($x$ = 6)), FN mobility is also seen to increase in direct proportionality to the increased mobility of the underlying polymer surface. These data, together with the AFM (Figure 4) and domain availability (Figure 5) results, indicate that the increasing mobility of the polymer surfaces (from $x$ = 2 to 6) compensates for the restricted motion within the FN network, without significantly altering the conformation of the protein.

**Effect of Mobility on Cell Behavior.** With cells responding to substrate-defined factors, like stiffness and topography,[1,4] it therefore stands to reason that this change in mobility, mediated through the protein layer, would affect cell behavior. Figure 7 shows how these factors can affect cell-mediated reorganization of the protein interface. The synthesis and reorganization of the ECM in vivo is known to be a tightly controlled and regulated system.[20] It is observed here that increased protein mobility allows cells to organize the protein network with greater ease in a similar to trend to that observed for the protein mobility despite minimal change in morphological cues (Supplementary Figure S4). Previous work has also observed increased cell-mediated organization with increased protein mobility.[27] Here increased protein mobility was achieved by reduction in adsorbed FN density as well as the interspersing of vitronectin with the system, both of which enhanced reorganization. It has also been observed that this interfacial mobility does not transfer through differential recruitment of integrins on each of these polymers (Supplementary Figure S5). This supports the hypothesis that the effect of mobility occurs on the picoscale.

C2C12 cells differentiate to different degrees on the four polymers. Maximal differentiation is observed on PEA ($x$ = 1) and PBA ($x$ = 4) surfaces, with significant increase noted compared with collagen (typical control material for myotube formation), PMA ($x$ = 1), and PHA ($x$ = 6). The difference in differentiation potential on these surfaces is accentuated by use of the myosin II inhibitor, blebbistatin.[41] With minimal changes in the nature of the protein network indicated in Figures 4 and 5 as well as the minimal changes in morphological cues observed on L929 cells (Supplementary Figure S4), it can be argued that the degree of interfacial mobility alters cellular behavior. These data can infer, not only, that the interfacial mobility of FN on the material surfaces increases the ability of cells to adhere and reorganize FN, but also that activation of cell contractility is required for mobility-dependent myotube formation. When cell contractility is inhibited, the less mobile surfaces produced greater levels of differentiation. This dependence of cell differentiation on surface mobility is in line with previous observations in mesenchymal stem cells on these polymers.[13] This, in conjunction with the minimal morphological differences of L929 cells, helps to demonstrate the effect of surface mobility on cell behavior.

## ■ CONCLUSIONS

It has been shown that fluorescence labeling of FN allows direct quantification of its mobility at the cell/material interface. A family of polyalkyl acrylates has been used, upon which FN is



DOI: 10.1021/acs.langmuir.5b03259
Langmuir 2016, 32, 800−809

organized into nanonetworks (at $x \geq 2$), so that there are no major differences in the initial state of the protein layer adsorbed on material surfaces. This work establishes that polymer mobility is translated into interfacial mobility of the adsorbed protein layer and that this, in turn, affects cell response. Indeed, the ability of cells to reorganize the protein layer is enhanced on the more mobile surfaces. It has been further shown that the sensing of mobility is related to cell contractility; this influences the ability of cells to differentiate on substrates of different interfacial mobility, altering the cell differentiation response.

## ■ ASSOCIATED CONTENT

### Supporting Information

The Supporting Information is available free of charge on the ACS Publications website at DOI: 10.1021/acs.langmuir.5b03259.

Static contact angles of the polymers, BCA assay of adsorbed FN, L929 morphological properties and focal adhesions analysis. (PDF)

## ■ AUTHOR INFORMATION


### Corresponding Authors

*E-mail: Manuel.Salmeron-Sanchez@glasgow.ac.uk.
*E-mail: Marco.Cantini@glasgow.ac.uk.


### Author Contributions

F.B., M.B., and M.C. contributed equally (in alphabetical order).

### Notes

The authors declare no competing financial interest.

## ■ ACKNOWLEDGMENTS

Financial support from ERC through HealInSynergy (306990) and MRC (MR/L022710/1) is acknowledged. EPSRC funding as part of the Doctoral Training Centre is also acknowledged. J.R. holds a Research Fellowship from the University of Glasgow. The help of Margaret O'Prey and her expertise in the confocal microscopy, from the BAIR, at the Beatson Cancer Research Institute is greatly appreciated.

## ■ REFERENCES


(1) Dalby, M. J.; Gadegaard, N.; Tare, R.; Andar, A.; Riehle, M. O.; Herzyk, P.; Wilkinson, C. D. W.; Oreffo, R. O. C. The control of human mesenchymal cell differentiation using nanoscale symmetry and disorder. *Nat. Mater.* **2007**, *6* (12), 997−1003.

(2) Kim, H. N.; Jiao, A.; Hwang, N. S.; Kim, M. S.; Kang, D. H.; Kim, D. H.; Suh, K. Y. Nanotopography-guided tissue engineering and regenerative medicine. *Adv. Drug Delivery Rev.* **2013**, *65* (4), 536−558.

(3) Yao, X.; Peng, R.; Ding, J. D. Effects of aspect ratios of stem cells on lineage commitments with and without induction media. *Biomaterials* **2013**, *34* (4), 930−939.

(4) Engler, A. J.; Sen, S.; Sweeney, H. L.; Discher, D. E. Matrix elasticity directs stem cell lineage specification. *Cell* **2006**, *126* (4), 677−689.

(5) Cukierman, E.; Pankov, R.; Stevens, D. R.; Yamada, K. M. Taking cell-matrix adhesions to the third dimension. *Science* **2001**, *294* (5547), 1708−1712.

(6) Trappmann, B.; Gautrot, J. E.; Connelly, J. T.; Strange, D. G. T.; Li, Y.; Oyen, M. L.; Cohen Stuart, M. A.; Boehm, H.; Li, B.; Vogel, V.; Spatz, J. P.; Watt, F. M.; Huck, W. T. S. Extracellular-matrix tethering regulates stem-cell fate. *Nat. Mater.* **2012**, *11* (7), 642−649.

(7) Chen, D.; Zhao, M.; Mundy, G. R. Bone morphogenetic proteins. *Growth Factors* **2004**, *22* (4), 233−241.

(8) Wen, J. H.; Vincent, L. G.; Fuhrmann, A.; Choi, Y. S.; Hribar, K. C.; Taylor-Weiner, H.; Chen, S.; Engler, A. J. Interplay of matrix stiffness and protein tethering in stem cell differentiation. *Nat. Mater.* **2014**, *13* (10), 979−987.

(9) Curran, J. M.; Pu, F.; Chen, R.; Hunt, J. A. The use of dynamic surface chemistries to control msc isolation and function. *Biomaterials* **2011**, *32* (21), 4753−4760.

(10) Liu, R.; Masters, K. S.; Gellman, S. H. Polymer Chain Length Effects on Fibroblast Attachment on Nylon-3-Modified Surfaces. *Biomacromolecules* **2012**, *13* (4), 1100−1105.

(11) Seo, J. H.; Kakinoki, S.; Inoue, Y.; Nam, K.; Yamaoka, T.; Ishihara, K.; Kishida, A.; Yui, N. The significance of hydrated surface molecular mobility in the control of the morphology of adhering fibroblasts. *Biomaterials* **2013**, *34* (13), 3206−14.

(12) Seo, J. H.; Yui, N. The effect of molecular mobility of supramolecular polymer surfaces on fibroblast adhesion. *Biomaterials* **2013**, *34* (1), 55−63.

(13) Gonzalez-Garcia, C.; Moratal, D.; Oreffo, R. O. C.; Dalby, M. J.; Salmeron-Sanchez, M. Surface mobility regulates skeletal stem cell differentiation. *Integr Biol-Uk* **2012**, *4* (5), 531−539.

(14) Kong, F.; Li, Z.; Parks, W. M.; Dumbauld, D. W.; García, A. J.; Mould, A. P.; Humphries, M. J.; Zhu, C. Cyclic Mechanical Reinforcement of Integrin−Ligand Interactions. *Mol. Cell* **2013**, *49* (6), 1060−1068.

(15) Balaban, N. Q.; Schwarz, U. S.; Riveline, D.; Goichberg, P.; Tzur, G.; Sabanay, I.; Mahalu, D.; Safran, S.; Bershadsky, A.; Addadi, L.; Geiger, B. Force and focal adhesion assembly: a close relationship studied using elastic micropatterned substrates. *Nat. Cell Biol.* **2001**, *3* (5), 466−472.

(16) Roth, C. B.; Dutcher, J. R. Glass transition and chain mobility in thin polymer films. *J. Electroanal. Chem.* **2005**, *584* (1), 13−22.

(17) Ellison, C. J.; Torkelson, J. M. The distribution of glass-transition temperatures in nanoscopically confined glass formers. *Nat. Mater.* **2003**, *2* (10), 695−700.

(18) Shattil, S. J.; Kim, C.; Ginsberg, M. H. The final steps of integrin activation: the end game. *Nat. Rev. Mol. Cell Biol.* **2010**, *11* (4), 288−300.

(19) Pankov, R.; Yamada, K. M. Fibronectin at a glance. *J. Cell Sci.* **2002**, *115* (20), 3861−3863.

(20) Cantini, M.; Gonzalez-Garcia, C.; Llopis-Hernandez, V.; Salmeron-Sanchez, M. Material-Driven Fibronectin Fibrillogenesis. In *Proteins at Interfaces III: State of the Art*; Horbett, T., Brash, J. L., Norde, W., Eds.; American Chemical Society: Washington, DC, 2012; Vol. *1120*, pp 471−496.

(21) Keselowsky, B. G.; Collard, D. M.; Garcia, A. J. Surface chemistry modulates fibronectin conformation and directs integrin binding and specificity to control cell adhesion. *J. Biomed. Mater. Res.* **2003**, *66* (2), 247−59.

(22) Vallières, K.; Chevallier, P.; Sarra-Bournet, C.; Turgeon, S.; Laroche, G. AFM Imaging of Immobilized Fibronectin: Does the Surface Conjugation Scheme Affect the Protein Orientation/Conformation? *Langmuir* **2007**, *23* (19), 9745−9751.

(23) Guerra, N. B.; Gonzalez-Garcia, C.; Llopis, V.; Rodriguez-Hernandez, J. C.; Moratal, D.; Rico, P.; Salmeron-Sanchez, M. Subtle variations in polymer chemistry modulate substrate stiffness and fibronectin activity. *Soft Matter* **2010**, *6* (19), 4748−4755.

(24) Gugutkov, D.; Altankov, G.; Hernandez, J. C. R.; Pradas, M. M.; Sanchez, M. S. Fibronectin activity on substrates with controlled -OH density. *J. Biomed. Mater. Res., Part A* **2010**, *92A* (1), 322−331.

(25) Schneider, C. A.; Rasband, W. S.; Eliceiri, K. W. NIH Image to ImageJ: 25 years of image analysis. *Nat. Methods* **2012**, *9* (7), 671−675.

(26) Leahy, D. J.; Aukhil, I.; Erickson, H. P. 2.0 A crystal structure of a four-domain segment of human fibronectin encompassing the RGD loop and synergy region. *Cell* **1996**, *84* (1), 155−64.

(27) Gonzalez-Garcia, C.; Cantini, M.; Moratal, D.; Altankov, G.; Salmeron-Sanchez, M. Vitronectin alters fibronectin organization at the cell-material interface. *Colloids Surf., B* **2013**, *111*, 618−25.




DOI: 10.1021/acs.langmuir.5b03259
*Langmuir* 2016, 32, 800−809

(28) Cantini, M.; Rico, P.; Moratal, D.; Salmeron-Sanchez, M. Controlled wettability, same chemistry: biological activity of plasma-polymerized coatings. *Soft Matter* **2012**, *8* (20), 5575−5584.
(29) Berglin, M.; Andersson, M.; Sellborn, A.; Elwing, H. The effect of substrate molecular mobility on surface induced immune complement activation and blood plasma coagulation. *Biomaterials* **2004**, *25* (19), 4581−4590.
(30) Garcia, A. S.; Dellatore, S. M.; Messersmith, P. B.; Miller, W. M. Effects of supported lipid monolayer fluidity on the adhesion of hematopoietic progenitor cell lines to fibronectin-derived peptide ligands for alpha5beta1 and alpha4beta1 integrins. *Langmuir* **2009**, *25* (5), 2994−3002.
(31) Salmeron-Sanchez, M.; Rico, P.; Moratal, D.; Lee, T. T.; Schwarzbauer, J. E.; Garcia, A. J. Role of material-driven fibronectin fibrillogenesis in cell differentiation. *Biomaterials* **2011**, *32* (8), 2099−2105.
(32) Baneyx, G.; Vogel, V. Self-assembly of fibronectin into fibrillar networks underneath dipalmitoyl phosphatidylcholine monolayers: Role of lipid matrix and tensile forces. *Proc. Natl. Acad. Sci. U. S. A.* **1999**, *96* (22), 12518−12523.
(33) Bergkvist, M.; Carlsson, J.; Oscarsson, S. Surface-dependent conformations of human plasma fibronectin adsorbed to silica, mica, and hydrophobic surfaces, studied with use of Atomic Force Microscopy. *J. Biomed. Mater. Res.* **2003**, *64A* (2), 349−356.
(34) Han, S. J.; Bielawski, K. S.; Ting, L. H.; Rodriguez, M. L.; Sniadecki, N. J. Decoupling Substrate Stiffness, Spread Area, and Micropost Density: A Close Spatial Relationship between Traction Forces and Focal Adhesions. *Biophys. J.* **2012**, *103* (4), 640−648.
(35) Discher, D. E.; Janmey, P.; Wang, Y.-l. Tissue Cells Feel and Respond to the Stiffness of Their Substrate. *Science* **2005**, *310* (5751), 1139−1143.
(36) Rape, A. D.; Guo, W.-h.; Wang, Y.-l. The regulation of traction force in relation to cell shape and focal adhesions. *Biomaterials* **2011**, *32* (8), 2043−2051.
(37) Anselme, K.; Bigerelle, M. Topography effects of pure titanium substrates on human osteoblast long-term adhesion. *Acta Biomater.* **2005**, *1* (2), 211−222.
(38) ter Brugge, P. J.; Wolke, J. G. C.; Jansen, J. A. Effect of calcium phosphate coating crystallinity and implant surface roughness on differentiation of rat bone marrow cells. *J. Biomed. Mater. Res.* **2002**, *60* (1), 70−78.
(39) Sipe, J. D.; Sipe, J. D.; Kelley, C. A.; McNicol, L. A. Tissue engineering and reparative medicine. *Ann. N. Y. Acad. Sci.* **2002**, *961*, 1−9.
(40) Lee, M. K.; Rich, M. H.; Lee, J.; Kong, H. A bio-inspired, microchanneled hydrogel with controlled spacing of cell adhesion ligands regulates 3D spatial organization of cells and tissue. *Biomaterials* **2015**, *58* (0), 26−34.
(41) Dillow, A. K.; Ochsenhirt, S. E.; McCarthy, J. B.; Fields, G. B.; Tirrell, M. Adhesion of alpha(5)beta(1) receptors to biomimetic substrates constructed from peptide amphiphiles. *Biomaterials* **2001**, *22* (12), 1493−1505.

## ■ NOTE ADDED AFTER ASAP PUBLICATION

This paper was published on the Web on January 7, 2016, with an incorrect Supporting Information file. The corrected version was reposted on January 8, 2016.



DOI: 10.1021/acs.langmuir.5b03259
*Langmuir* 2016, 32, 800−809